SMART Rotor Development and Wind Tunnel Test

Friedrich K. Straub
Boeing Technical Fellow
The Boeing Company
Mesa, Arizona

Vaidyanathan R. Anand
Dynamics Engineer
The Boeing Company
Mesa, Arizona

Terrence S. Birchette
Design Engineer
The Boeing Company
Mesa, Arizona

Benton H. Lau
Aerospace Engineer
NASA Ames R.C.
Moffett Field, California

ABSTRACT

Boeing and a team from NASA, Army, DARPA, Air Force, MIT, UCLA, and U. of Maryland have successfully completed a wind tunnel test of the smart material actuated rotor technology (SMART) active flap rotor in the 40- by 80-foot wind-tunnel of the National Full-Scale Aerodynamic Complex at NASA Ames Research Center. The Boeing SMART active flap rotor is a full-scale, five-bladed bearingless MD 900 helicopter rotor modified with a piezoelectric-actuated trailing edge flap on each blade. The eleven-week test program evaluated the forward flight characteristics of the active-flap rotor at speeds up to 155 knots, gathered data to validate state-of-the-art codes for rotor aero-acoustic analysis, and quantified the effects of open and closed-loop active flap control on rotor loads, noise, and performance. The test demonstrated on-blade smart material control of flaps on a full-scale rotor for the first time in a wind tunnel. The effectiveness of the active flap control on noise and vibration was conclusively demonstrated. Results showed reductions up to 6dB in blade-vortex-interaction and in-plane noise, as well as reductions in vibratory hub loads of about 80%. Trailing-edge flap deflections were controlled with less than 0.2 deg rms error for commanded harmonic profiles of up to 3 deg amplitude. The impact of the active flap on control power, rotor smoothing, and performance was also demonstrated. Finally, the reliability of the flap actuation system was successfully proven in more than 60 hours of wind tunnel testing.

INTRODUCTION

Vibration, noise, and aerodynamic design compromises are inherent barriers to significant improvements in effectiveness, productivity, and public acceptance of the helicopter. Specific rotary-wing challenges include cyclic variations in free stream velocity, blade controls and motions, transonic flow on the advancing side, reversed flow and dynamic stall on the retreating side, blade/vortex interaction (BVI), blade/fuselage flow interactions, swashplate mechanical constraints, and flight control hydraulic actuator bandwidth.

Passive design techniques, such as optimized airfoils, tip shapes, tuned blade structures, etc. are successful in providing incremental gains. Still, in many cases operational restrictions are necessary to mitigate the noise impact, vibration absorbers are required to reduce vibrations, and aerodynamic performance in various mission segments is compromised by the constraints on blade design.

Numerous active control concepts have been investigated that effect rotor blade motion or shape at frequencies above 1/rev in order to mitigate unsteady effects, or adapt the blade to mission segments with conflicting design requirements. Higher harmonic control (HHC) through the swashplate [1,2], individual blade control (IBC) at the blade root [3-7], and trailing edge, active flap control (AFC) on the blade [8,9] have been successfully flight tested. Significant reductions in vibrations of about 80%, in BVI noise during descent of about 5dB, and in rotor power during high speed level flight of about 6% were demonstrated. Similar results have also been reported from numerous model and full-scale rotor wind tunnel tests.

On-blade active control using smart materials has recently been applied in a number of model scale [10-16] and full-scale rotor experimental programs [8,17,18]. Piezoelectric materials are used for high frequency actuation at small amplitudes. Some of the model rotor programs [13,14] used distributed piezo fibers to effect elastic twist actuation of the blade. All of the full-scale rotors used discrete piezo actuators and trailing edge flaps. This approach offers a number of advantages compared with HHC and root pitch IBC. The undesirable loading is suppressed at the source, requiring less actuation power. The system can be tailored to the blade aeromechanics through spanwise placement and even multiple flaps [8,19]. It is independent of the primary flight control system, not constrained by the swashplate, and uses electric power. Solid state piezoelectric actuators have high bandwidth and a minimum of moving parts.

Presented at the 35th European Rotorcraft Forum, Hamburg, Germany, Sept. 22-25, 2009.

Modeling of rotors with on-blade controls has seen increased activity in recent years. A comprehensive assessment of six different on-blade control schemes and IBC for performance enhancement [20] used the comprehensive code CAMRAD II [21]. Simultaneous reductions of vibration and noise as well as vibration and rotor power for active flap rotors were shown to yield suboptimal results in the individual objectives [22,23]. Most recently, a coupled CFD-CSD code has been applied to model the SMART active flap rotor [24]. Correlation with the data reported here has shown improved prediction of cyclic flap bending and torsion moments over comprehensive codes, and the ability to capture 3-dimensional flow effects at the edges of the active flap. Correlation of CMARAD II predictions with the SMART rotor data set [25] has shown reasonable results for flap bending moment and pitch link load, but also shown the need to further refine the blade structural/inertia properties of the model.

Under a joint DARPA/NASA/Army-funded program, Boeing and a team from the Air Force, NASA, Army, DARPA, Massachusetts Institute of Technology, University of California at Los Angeles, and University of Maryland have recently completed a successful wind tunnel test of the SMART active flap rotor in the Air Force National Full-Scale Aerodynamic Complex (NFAC) 40- by 80-foot anechoic wind tunnel at NASA Ames Research Center. The eleven-week wind tunnel test program evaluated the forward flight characteristics of the full-scale active flap rotor, gathered data to validate state-of-the-art codes for rotor aero-acoustic analysis, and quantified the effects of open- and closed-loop active-flap control on rotor loads, noise, and performance.

The present paper briefly describes the SMART rotor development and hardware. It focuses on the wind tunnel test program, test setup, and provides an overview of test results.

SMART ACTIVE FLAP ROTOR

The Boeing SMART rotor, developed under the sponsorship of DARPA, NASA, Army, and internal funding, is a MD 900 helicopter (see Fig. 1a) full-scale, five-bladed bearingless rotor, modified with piezoelectric-actuated trailing edge flaps on each blade (see Fig. 1b). The objective of the development of this rotor system was to demonstrate significant rotor-induced vibration and BVI noise reductions and aerodynamic performance improvements in wind tunnel and flight tests. The development effort included design, fabrication, and component testing of rotor blades, trailing edge flaps, piezoelectric actuators, switching power amplifiers, actuator control system, and the data/power system. Development of the SMART rotor culminated in a whirl tower test in 2003 (see Fig. 1c), which demonstrated the functionality, robustness, and required authority of the active flap system [18]. Additional details on the design, development and testing of this active flap rotor system are provided in [26].

The SMART rotor is a 33.85-ft diameter (blade radius, R of 203.1 inches), full-scale, bearingless, five-bladed main rotor modified from the MD 900 Explorer rotor system. Each blade consists of 12% thick HH-10 airfoil sections inboard up to 74% radius and 9.5% thick HH-06 airfoil sections outboard beyond 84% radius, with a linear twist of –10 degrees. The blade tip region, from 93% radius to the tip has a parabolic leading edge sweep (22 degrees at the tip), straight trailing edge and a 2:1 taper ratio. The constant chord section of the blade has a 10 inch chord. Nominal rotation speed of the rotor is 392 RPM producing a tip speed of 695 ft/sec. At 5,811 pounds thrust, the rotor thrust coefficient normalized by thrust-weighted rotor solidity is 0.075 at sea level standard conditions. Rotor properties are summarized in Table 1.

Of particular interest here is the design of the flap system and its integration into the MD 900 rotor blades. Aerodynamic and aeroelastic simulations were conducted early on [27] to define the flap type, flap chord and flap span such that the flap system has enough control authority to provide required dynamic lift variations for vibration and noise reduction and requires the minimum actuator power. The flap system selected has a flap chord of 25% (hinge to trailing edge) with an overhang of 40% (total flap length of 35% chord) and flap span of 18% rotor radius with its center located at 83% rotor radius to provide required control authority while minimizing the flap hinge moments [26]. The flap is mounted to the blade using five equally spaced hinges to minimize stresses (see Fig. 1c). Its amplitude is mechanically limited to 6 deg. Flap properties are summarized in Table 2.

Each blade contains an embedded 2x-frame actuator with four piezoelectric stack columns (see Fig. 1d) [28], designed to drive the trailing edge flap at frequencies up to 11-per-rev (11P) with as much as 4 deg amplitude authority under load. Each actuator is powered by a 2-channel switching power amplifier. The piezo stacks are driven by a DC bias voltage and a dynamic voltage. The dynamic voltage for the outboard x-frame is 180 deg out-of-phase relative to the voltage for the inboard x-frame actuator. In this paper, references to voltage refer to the dynamic voltage only. Actuator properties are shown in Table 3. Inputs to the five actuators are controlled using a PC-based system. Typically, inputs

are phased azimuthally such that each flap receives the same command at a given azimuth. The flap deflection for the k^{th} blade is

$$\delta_{fk} = A_n \sin (n \psi_k + \phi_n), \quad n = 0 \quad 1$$

$$\text{where} \quad \psi_k = \psi_1 - (k\text{-}1)\, 2\pi/5, \quad k = 1\text{-}5.$$

Positive flap deflections are trailing edge down. For the rest of this paper, active flap settings will be described in a three-parameter form, $A_n/nP/\phi_n$ – where amplitude A_n and phase ϕ_n are expressed in degrees, n is an integer multiple of the non-dimensional rotor speed, and P stands for per rev.

The piezoelectric actuator is installed in the blade spar at 74% radius. It drives the flap via a linkage that is connected to a horn at the inboard end of the flap (see Fig. 1e). A comparison of SMART and MD900 blade mass properties shows that the flap/actuator system increases blade weight by about 5 lb (see Table 4). A comparison of SMART and MD900 blade modal frequencies for computed rotating and measured free-free conditions is shown in Table 5. In the analysis, the test stand control system stiffness was used for both rotors, and the active flap was locked out. Results show that the design goal to match SMART blade dynamics to the baseline blade was achieved. In particular it should be noted that no effort was made to lower the blade torsional stiffness and thus increase the active flap effectiveness. Also shown is the fundamental mode of the actuator/flap (1TEF) when installed in the blade at about 96 Hz.

WIND TUNNEL TEST SETUP

Large Rotor Test Stand

In preparation for the wind tunnel entry, a brief whirl tower test was conducted (see Fig. 2). This system integration test verified operation of the SMART rotor, large rotor test stand (LRTS), rotor control console (RCC), test stand health monitoring system (HMS), flap actuator power amplifier and control system, and data acquisition, processing, and display systems.

Boeing's LRTS1 (Fig. 2), consists of a sled structure that supports a 1500-hp General Electric motor, 1500-hp gearbox, and tail sting. A vertical main strut is mounted to the gearbox and supports the balance housing, balance, static mast, hydraulic actuators, swashplate, and rotor. The static mast encloses the final drive shaft that transfers torque to the rotor hub. Two horizontal outrigger arms attach to the main strut just above the gearbox. The entire stand is mounted to a tripod support. The LRTS was previously used during the MDART (MD900 pre-production rotor) 40- by 80-ft wind tunnel test entry [29].

When installed in the NFAC 40- by 80-foot wind tunnel test section, the LRTS is mounted on a three-strut support system placing the rotor hub 23.7 ft above the tunnel floor at zero degree shaft tilt (see Fig. 3a). The LRTS outrigger arms are mounted to two fixed, faired struts via ball joints and the tail sting is mounted to an extensible tail strut that provides shaft tilt. Three sets of fairings are used to enclose the sled/motor/gearbox, the main strut, and the balance/controls.

Instrumentation

Blade load measurements include 6 flap, 4 chord and 4 torsion moments at various radial stations, as well as one set of flap, chord, torsion moments each on the pitchcase and flexbeam of this bearingless rotor. Pitch link load and drive shaft torque are also measured. The piezoelectric actuator stroke and force are measured on each blade. Piezo stack temperature and active flap lift load at two intermediate hinges are measured on one blade. All rotating system measurements are acquired and multiplexed in a hub-mounted data system (see Fig. 3b). The multiplexed data and the actuator control power are transmitted through a conventional 36-channel slip ring. Test stand measurements include hub accelerations, static mast bending, the five-component rotor balance, swashplate actuator motions, optical shaft encoder, and numerous test stand health parameters. Wind tunnel test conditions are measured using a redundant set of analog as well as digital sensors.

For acoustic measurement, a series of microphones was strategically placed around the model to capture rotor noise sources of interest (see Fig. 4a). These microphones were grouped into: a) out-of-plane fixed microphones (M1 and M4) to correlate to microphones used previously in the MDART test [29] b), traverse microphones (M5 through M12) that can be moved along guided rails for blade-vortex interaction noise mapping, c) in-plane microphones (M13, M15 and M14) for low frequency, in-plane rotor noise measurement, and d) fixed microphone (M16) on the rotor balance fairing. Microphones M13, M15 and M14 were mounted on tower struts to be near in-plane of the rotor (approx. 10 degrees below wind tunnel horizon). With the exception of M14, all microphones are located within the acoustically-treated portion of the 40- by 80-foot test section. The microphone traverse travel ranges from 200 inches upstream of the center of the rotor hub to 200 inches downstream with traverse stopping at every 40 inches. The plane of traverse microphone positions is located 89.4% radius below the rotor hub center, extends from 41% to 141% radius across the test section on the advancing side, and from 98.5% radius upstream to 98.5% downstream. A top view of the microphone layout is shown in Fig. 4b, and additional details are provided in two companion papers [30, 31].

Active Flap Control

The flap actuator high-voltage power amplifiers and PC-based controller are located in the control room. The user interface for providing control inputs and monitoring execution is developed using dSPACE ControlDesk software. The open and closed-loop control laws are implemented on a dSPACE DS1103 single-board controller. The board has 20 channels of analog input, 8 channels of analog output, and other digital I/O channels and external interrupt inputs. A dedicated Simulink blockset is used to simplify development of real-time controllers in the MATLAB/Simulink environment. Rotor azimuth angle is determined from 1/rev and 512/rev signals provided by the optical encoder. The commanded actuator voltages output from the dSPACE controller are amplified by high-voltage amplifiers, and the resulting actuator signals are passed via the test stand slip ring into the rotating frame and to the individual actuators. One active flap command voltage, actual voltages and currents on all flap actuators, and amplifier power supply voltage and current are measured.

The active flaps are controlled in one of three modes. For open-loop control, actuator voltage is specified and no feedback from the rotor is used. For closed-loop position control, the flap deflection is specified in degrees, and feedback loops are closed on 5 actuator strokes, which are kinematically related to flap deflections. Either a continuous time higher harmonic controller (CTHHC) [32] or a modified version of the discrete time controller (HHC) from [33] is used. For closed-loop control of vibratory hub loads, rotor balance loads are used for feedback with the CTHHC controller.

Data Acquisition and Processing

Data channels from the rotating portion of the model in the tunnel (blades, hub, pitch links, flaps, etc.) are combined on the hub by a Metraplex Mini 770 data acquisition system into a pulse code modulated (PCM) serial data stream, and transmitted through one of the slip ring channels into the fixed frame to the control room. Data channels from the non-rotating portion of the model (test stand, balance, etc.) are combined in the control room with flap actuator and amplifier voltage and current measurements, rotor RPM and azimuth, the wind tunnel operating condition analog measurements, and four microphones (M1,4,13,16) by another Metraplex Mini 770 system into a second, non-rotating PCM data stream.

Both PCM data streams are time-based and recorded continuously on Boeing's data system. Key parameters are displayed in various formats on four flat panel displays and two 18-channel electronic strip charts for real time monitoring. Test stand HMS data is monitored and recorded on a dedicated system. Typically 12 sec of data are post-processed per test point; for active flap frequency sweeps and closed-loop vibration control points, 40 sec are used. All acoustic data and wind-tunnel operating conditions are recorded by the azimuth-based NFAC wind-tunnel data system, using 10 sec per point (within the 12 sec of Boeing data). The NFAC acoustic data acquisition and reduction system enabled the near real-time acoustic processing of the data. After the tests, both data sets are aligned using a triangular wave form alignment signal and rotor azimuth.

When post-processing steady-state test points, sixty-four revolutions of data (approximately 9.75 seconds) are used. All channels, except acoustic measurements, are re-sampled to 256 samples/rev on an azimuth basis. The acoustic data channels are digitized at an effective sampling rate of 2048 samples/rev (equivalent to 13,380 samples/sec at the nominal 392 RPM). The data exhibited good rev-to-rev repeatability; therefore, a straightforward synchronous average of the time history data resulted in an averaged time history of one revolution duration of 256 or 2048 points.

A hub weight tare, rotation tare, and aerodynamic tare were taken before the test, in the configuration used during the test, except that the blades were replaced by spacers placed inside the pitchcase to firmly restrain the flexbeam tips. During the weight and rotation tare, the test section overhead and access doors were open. A blade weight tare was taken before and after the test. The rotor was balanced and tracked using an Advanced Vibration Analyzer (AVA) and optical strobe. No commands were made to the active flaps. Final balance was about 0.1 in/sec and track was well within one chord thickness at the tip.

TEST OBJECTIVES AND APPROACH

The 11-week long wind-tunnel test was sponsored by DARPA, NASA, and the U.S. Army. The objectives of the DARPA-funded portion of the test were to acquire loads, performance, and acoustic data for an advanced rotor system in support of validating high-fidelity physics-based rotor noise prediction tools that had been developed under the Helicopter Quieting Program (HQP).

Test conditions for the validation data base included level-flight, descent, and high-speed cases with single and multiple harmonic flap inputs. Four test points were defined with speeds of 83, 123, and 155 knot, (see Table 6, Validation, condition 1-4). For each point the velocity, advancing tip Mach number, shaft angle, blade loading, the baseline (0 deg) and a flap deflection

schedule were specified. Flap inputs included amplitudes up to 3 deg at specified phasing and 2, 3 or 5/rev harmonic variation. All predictions were completed before the test, and therefore flap position control was used to closely follow the specified flap deflections. Data was successfully acquired at three test points. Blade loads were too high for the high-speed condition at 155 knot to exercise the specified flap deflection schedule, however, baseline data (with zero degree flap deflection) was acquired.

The primary objectives of the NASA-funded portion of the test were to evaluate the effect of open and closed-loop active flap control on BVI noise, in-plane noise, and vibratory hub loads. Secondary objectives were control power, rotor smoothing, and performance, (see Table 6), as well as rotor dynamics and flight control system identification from active flap frequency sweeps. Test conditions included hover, descent and level flight cases at 62, 68, 82, and 124 knots. For each test point advance ratio, tip Mach number, shaft angle, and blade loading were specified. The advance ratio and tip Mach number specified are based on the specified level flight speed, nominal rotor tip speed, and sea level standard day conditions.

For noise reduction, single harmonic flap inputs at 2 to 5/rev with fixed amplitude (typically 1.5 deg) and phase sweeps (0 to 360 deg in 30 deg increments) were used to determine the optimum phase angle. Amplitude sweeps at optimal frequency and phase were then used to further reduce noise. For all noise test points, feedback of the actuator position was used to control the flap deflections precisely. For vibration reduction, open-loop flap control at 2 to 6/rev with 250V amplitude and phase sweeps were used to establish controllability. Closed-loop vibration control used the CTHHC controller with feedback of rotor-balance normal force, roll, and pitch moment (NF, RM, and PM).

The effectiveness of the active flap for control power was evaluated using position control at 0 and 1/rev with amplitudes of -3 to 3 deg and appropriate phasing. Flaps were controlled either individually, specifying harmonic and phase (IBC), or through software implementation of a virtual swashplate (VSP), using amplitude and collective, longitudinal, and lateral cyclic commands. The effectiveness of the active flap for rotor smoothing (i.e. blade tracking) was evaluated using position control with steady flap amplitudes of -3 to 3 deg on a single flap, either flap 1 or 2. The effectiveness of the active flap for rotor performance improvements was evaluated using position control at 2/rev with 1.5 deg amplitude and phase sweeps. Rotor dynamics (modal identification) and flight controls (rotor response) were investigated by performing open-loop flap linear and logarithmic frequency sweeps up to 80 or 200Hz or around rotor speed multiples of interest. Amplitudes of 150, 175, and 200V and the VSP collective, longitudinal, and lateral cyclic inputs were used.

For each test condition the rotor was trimmed to the desired thrust and minimal rotor flapping as determined from flexbeam cyclic flap bending. After trimming at the baseline condition, unless noted, the rotor was not retrimmed during subsequent flap phase and amplitude sweeps or microphone traverse.

TEST RESULTS

A sample of test results covering all the objectives is presented here. Detailed results for the BVI noise, in-plane noise, vibration reduction, and flap position control are shown in the companion papers [30, 31, 32]. All test results shown here were obtained at a nominal thrust coefficient-to-solidity ratio (C_T/σ) of 0.075 (which corresponds to 5811 pounds of rotor thrust at sea level, standard day conditions). Exceptions were hover cases, typically run at θ = 4 deg blade collective pitch and 10 deg forward shaft tilt to reduce recirculation, and the performance data with 2/rev inputs.

Position Control

One of the goals of the wind tunnel test program was to precisely control blade flap position in a number of specific flight conditions, to allow for correlation of wind tunnel acoustic data with pretest predictions of rotor aeroacoustics. Analysis of an early SMART rotor configuration in forward flight has shown that flap dynamics can result in considerably larger than open-loop commanded flap deflections in the first quadrant [34]. Furthermore, SMART whirl tower data has shown differences in the open-loop active flap response on each blade [35], possibly due to the combined effects of flap rigging, flap control system stiffness, and piezoelectric actuator performance. Thus, the need for closed-loop flap position control was indicated. All results shown here were obtained with the CTHHC controller. It was based on the actuator voltage to flap position transfer function, identified from frequency sweep data at 82kt, and controls harmonics 0-6/rev [32]. A single controller was used for all test points, since the transfer function was essentially invariant with flight condition.

For the wind tunnel test, the flap rigging (Ω=0) was very tightly controlled to within 0.1deg for 5 flaps, (see Fig. 5a). In addition, it is noted that the nonrotating actuator/flap fundamental frequencies are within 2.5% of their average value (not shown). Figure 5a shows the flap deflection (min, max, and average of 5 flaps) versus

speed for the uncontrolled case (0V), that is no voltage going to the flap actuators. The aero/inertia loading deflects the flaps from -0.5 to 3 deg, with the range of values increasing with speed. Figure 5b shows that for closed-loop flap position control with a 0 deg command, flap deflections are maintained within ±0.12 deg from 0 deg. The largest error is seen at the 62kt descent condition, possibly a result of BVI. For harmonic flap commands (Fig. 5c), the mean flap position is well within ±0.1 deg from 0 deg and the largest rms error of 0.2 deg occurs for the 2 deg 5/rev command at 124 kt. Figures 5b-c show that the CTHHC controller was very effective in controlling flap position. Similar results were seen for the HHC controller using on-line identification and harmonics 0-5/rev.

Flap deflection time histories for three cases are shown in Figures 6a-c. The uncontrolled case (0V, Fig. 6a) illustrates the differences between 5 flaps and significant effect of aero/inertia loading on flap deflections around 90 deg azimuth. The harmonic flap deflections in Figures 6b-c illustrate the fidelity in matching commanded flap deflection profiles. Small differences are seen from flap to flap and for 5/rev the error at peak flap deflection may be as large as 0.4 deg.

Rotor and Active Flap Dynamics

Data was collected for about 200 active flap frequency sweeps (chirps) in hover, 82, and 124 kt. Open-loop flap inputs were made using collective, longitudinal, and lateral cyclic modes. Sweep range from 0-200 Hz was used for flap actuator dynamics. A range from 0-80 Hz was used for rotor dynamics, and 0-9 Hz was used for flight controls. Close-up sweeps were conducted spanning (n±1/2)/rev for harmonics 2-6 and 10. Figure 7 shows pitchcase torsion response in hover to a 0.2-80 Hz sweep with logarithmic rate and 200V collective amplitude. The blade fundamental torsion mode is readily seen at about 5.8/rev in the power spectral map and phase plot.

Phasing of the active flap angle (+ TE down) relative to actuator voltage, and flexbeam flap bending (+ up) and flexbeam torsion (+ LE up) relative to flap angle are shown in Figures 8a-b for 82 and 124kt respectively. These are obtained from active flap excitation and responses at integer harmonics. Phase lead is positive. Figure 8a (=0.2) shows that the flap deflection lags the voltage by about 20 degrees across the entire range. The phase of flexbeam torsion to active flap decreases gradually from 180 deg at 0/rev to about 40 deg at 6/rev. It crosses 90 deg between 5 and 6/rev, near the blade torsion mode. The phase of flexbeam flap bending to active flap is 180deg at 0/rev and decreases rapidly with increasing frequency as the three flap bending modes are crossed. Very similar results are seen in Fig. 8b for =0.3.

From the above it is clear that the active flap affects overall blade response via the moment, or servo, effect. At frequencies below the torsion mode, flap down deflection increases lift at the trailing edge which results in a nose down pitching moment and blade torsion response, and thus reduced section lift. Above the torsion mode the blade torsion response reverses. Blade flapping at 0 and 1/rev responds to the reduced lift as expected with down flapping (about 90 deg phase lag relative torsion at 1/rev). At higher frequencies, the blade flapping response changes phase rapidly and examination of flap bending and torsion at outboard stations, where the flap affects local airloading, may be required to better understand the flapping response and its impact on noise and vibration. Unsteady aerodynamics also plays a role, however, unsteady lift is not expected to add more than 20-30 deg phase lag.

BVI Noise Reduction

High noise levels in helicopter descent or maneuvers are caused by an impulsive noise-generating mechanism known as blade-vortex interaction (BVI) that results from the close proximity between the main rotor blades and the vortices generated by them. BVI noise radiates out-of-plane and is the primary source of noise annoyance around heliports when the rotor is close to the ground during landing approach. BVI noise can be reduced by redistributing airloads near the blade tip to reduce the tip vortex strength in the 2nd quadrant or by increasing the vertical separation (miss distance) between the blade and the tip vortex during the interaction.

Effects of the active flap on BVI noise were evaluated at three descent flight conditions with =0.15, 0.165, and 1 0.2. Shaft angle sweeps were conducted for the baseline rotor (0V flap command) to identify the shaft angles corresponding to maximum BVI. For condition 2 the shaft angle was estimated at 1.8 deg aft for the 6 deg glide slope used during MD900 FAA certification, and rotor speed was set at 392 rpm. All subsequent BVI noise test points were obtained with flap position control. A traverse sweep for the baseline rotor (simulated with flap position at 0deg) was then conducted to identify the microphone location with the highest BVISPL. BVISPL was determined from the band-pass filtered spectrum between blade passage harmonics 8-60. The optimum combination of active flap parameters for BVI noise reduction at the selected location was then determined through systematic phase, frequency, and amplitude sweeps. For additional details see [30].

Figure 9 shows the change in BVISPL from baseline for microphone M7 at traverse station -120 as a function of flap phase, with 1.5 deg amplitude at single harmonics 2-5 (condition 1, =0.15, α=4˚). Noise reductions from 3 to 6 dB are seen at the best phase for each of the four harmonics. An amplitude sweep from 1 to 2 deg at the best frequency and phase combination of 4P/30˚ determined that active flap actuation of 1.5˚/4P/30˚ provided best BVISPL noise reduction at all microphones at this traverse location.

A traverse sweep was conducted with the 1.5˚/4P/30˚ flap actuation. Figure 10a shows the carpet plots of BVISPL contours for the baseline rotor, rotor with 1.5˚/4P/30˚ flap actuation, and the difference (active flap rotor noise levels minus the baseline rotor noise levels) in noise levels between the two. BVISPL values used in these contours are averaged over repeat data points where available. Figure 10a clearly shows that the active flap was able to reduce the BVI noise over a wide range of directivity angles under the advancing side with BVISPL reductions as high as 7 dB. With active flap, the BVISPL at the baseline hot spot location was reduced by as much as 3.5 to 6 dB. Figure 10b shows the time history and spectral data comparisons between the baseline rotor and the rotor with 1.5˚/4P/30˚ flap actuation for microphone M7 at traverse station -120. Figure 10b clearly shows the reduced acoustic pressure and higher harmonic spectral levels with flap actuation resulting in 7.1 dB reduction in BVISPL relative to the baseline, thus demonstrating the effectiveness of harmonic flap actuation for reducing BVI noise. However, this active flap actuation which produced large BVI noise reductions also produced large increases in vibratory hub loads relative to those for the baseline rotor.

Similar results [30] were obtained for the simulated FAA noise certification descent flight (μ=0.165). A flap schedule of 1.5˚/3P/180˚ was able to reduce BVI noise levels by as much as 5 dB. Noise reductions at the baseline rotor BVI hot spot locations varied between 3 and 5 dB. For the moderate high speed test case (μ=0.2), a flap schedule of 1.5˚/3P/180˚ produced smaller BVISPL reductions, with a maximum of about 3 dB.

In-plane Noise Reduction

Low frequency rotor harmonic tones, emitted from near in-plane of the rotor, are particularly of concern for military operations, as they tend to propagate long distances without substantial attenuation by atmospheric absorption. At positions near in-plane and forward of the rotor, the radiated noise is primarily due to thickness and in-plane loading mechanisms. Because the directivity of the in-plane loading noise nearly matches the directivity characteristics of thickness noise near in-plane of the rotor, it was proposed to use on-blade controls to alter blade airloads and generate an in-plane loading noise profile that would negate or reduce the thickness noise pulse [31]. Achieving this "anti-noise" profile would require an increase in the in-plane loading as the blade approaches the advancing side near 90˚ blade azimuth.

Effects of the active flap on in-plane noise were evaluated for a level flight condition (=0.3, α=-9.1˚), considering microphone M13 and a low frequency sound pressure level (LFSPL) noise metric, which includes acoustic energy only in the first six blade-passing harmonics. All test points were obtained with flap position control.

Figure 11a shows the change in LFSPL from baseline for microphone M13 as a function of flap phase, with 1.5 deg amplitude at single harmonics 2, 3, and 5P. Only a 1 deg flap amplitude was realized for the phase sweep at 4P due to high blade loads. Noise reductions from 4 to 5 dB are seen at the best phase for each of the four harmonics. Amplitude sweeps from 0.7 to 2 deg for the best frequency and phase combinations 2P/0˚, 3P/250˚, and 4P/180˚ were conducted to further explore the effectiveness of the active flap. Within this range of flap amplitudes, Figure 11b shows that increasing flap amplitudes at 3P and 4P achieved more noise reductions. Best noise reduction of 5.1 dB and 5.7 dB was achieved at 2.0˚ flap amplitude at 3P, and at 1.3˚ flap amplitude for 4P, respectively. Beyond these measured flap amplitudes, extrapolated trends suggest that there is an optimum point whereby a further increase in flap amplitude does not necessarily result in more noise reductions. This is shown to be the case for 2P where noise reduction margin diminishes from 2.8 dB at 1.5˚ flap amplitude to 2.0 dB at 2.0˚ flap amplitude.

Examination of the active flap motion and blade torsion moment at 0.82R showed that all reduced-noise conditions exhibit decreasing active flap deflection (maximum flap up rate) near 90˚ azimuth, while simultaneously the blade twists LE up [31]. It was concluded that reduced noise was likely due to active flap induced changes in aerodynamic loading and blade torsion response at the blade tip near 90˚ azimuth. The net effect was to increase in-plane blade forces towards the trailing edge and thereby reduce in-plane noise. Not surprisingly then, reduced noise was accompanied by an increase of in-plane hub loads at 5/rev.

The underlying mechanism of these reduced in-plane noise levels is illustrated for the three best cases from Figure 11b. Figure 12 shows the ability of the active

flap to change in-plane loading and thus generate appropriate "anti-noise" pulses that partially cancel the 1 negative pressure peak commonly associated with steady thickness noise, and thereby reduce the net acoustic radiation forward of the rotor [31]. Active flap control was found to reduce negative acoustic pressure peaks by at least 50%. These reductions, however, did not occur uniformly for the pulses emanating from all five blades. Compared to the baseline acoustic signature, as well as the more benign 2P case, actuating the trailing-edge flap at 3P and 4P appear to generate much stronger blade-to-blade differences.

Vibration Reduction

The source of rotor-induced helicopter vibration is the unsteady environment experienced by the blades. The unsteady blade forces are then transmitted through the hub to the fixed frame, and are felt as vibration in the fuselage. Generally, the forces on the blades are harmonics of the rotor frequency, Ω, since the rotor aerodynamics are (nearly) periodic. Theoretically, only those harmonics that are multiples of the fundamental frequency at iN and iN±1 (where N is the number of blades and i is an integer) produce vibration in the fixed frame, due to the symmetry of the rotor. However, in practice, all harmonics contribute to vibration, due to asymmetries in the rotor, such as blade-to-blade imbalance and tracking error.

Both open-loop (voltage command) and closed-loop control using CTHHC were applied. Assuming that the effects of rotor dynamic periodicity are small and can be neglected, the input-output relationship between controls and rotor loads should be time-invariant and approximately linear. In that case, classical, discrete-time HHC [36] can be extended to obtain a continuous time higher harmonic controller (CTHHC) of the form

$$K_n(s) = 2/T_n \, (A_n s + B_n n\Omega) / (s^2 + (n\Omega)^2)$$

where n is the harmonic to be controlled, T_n is the desired time constant of the control loop, and A_n and B_n are constants obtained from off-line identification of an appropriate rotor transfer function. The benefits of this approach are generally better phase and gain margins and the ability to use classical control techniques to evaluate performance and stability. If from the Nichols plot it turns out that the choice of time constant T_n for any of the controlled harmonics results in low gain or phase margins, one or more of the time constants may have to be increased in order to achieve acceptable margins. In addition, the controller uses an integral term $K_0(s) = A_0 / (T_0 s)$ to control steady forces or displacements, and a modulation/demodulation scheme to track small variations in rotor speed.

The effectiveness of the active flap to modify the aerodynamic loading and reduce vibratory hub loads was evaluated at two flight conditions, descent (=0.2, α=21deg) and level flight (=0.3, α=-9.1 deg). Open-loop active flap control phase sweeps were conducted at both conditions with 250V amplitude for a single harmonic from 2-6P in order to establish control sensitivity. Figure 13 shows the sine and cosine 5P balance loads at =0.3 for 4, 5 and 6P inputs with points forming a circle as phase is swept from 0 to 360 in 30 deg increments. Baseline (0V) loads are also shown, generally near the middle of the circle. The larger the circle, the more sensitive the load is to the specific input harmonic. From this it is clear that 6P is least effective while 4P is most effective. For the normal force 5P is as effective as 4P, however somewhat less so for the other loads. Not shown, 2P was about as ineffective as 6P, while 3P was more effective than 5P for the in-plane forces and the moments. For 4P and 5P the circle encloses the origin for all loads, indicating that any single load can be zeroed out with a moderate voltage.

Also shown in Figure 13 are results for a vibration index, which is a weighted sum of the squared 5P balance loads. From the plot of vibration index magnitude versus phase, it is clear that control of multiple loads simultaneously with a single harmonic is not effective, because of the different phases required to zero out different loads.

Closed-loop vibration control used feedback of a single balance load at a time. At =0.2 normal force and roll moment at 5, 1, or 1-5P were used; at =0.3 balance normal force at 1-5P or 10P and pitch moment at 1-5P were used. Active flap frequency sweeps were conducted at both conditions using collective, longitudinal, and lateral cyclic inputs to acquire the data needed to identify the transfer functions and determine the controller constants [32].

Figure 14a shows the spectrum (i.e. magnitude of the fast Fourier transform) of the balance normal force for =0.2, α=2 1deg. Arbitrary units are used, since the magnitude depends on the number of samples in the FFT. There are significant impulses in the spectrum at all the integer harmonics from 1-11P, except 8P. This indicates the presence of some asymmetry in the rotor, due to blade-to-blade differences, rotor track and balance, or non-rotor induced loading. Also, there is a slightly broadened peak at about 6.2/rev, which is a transmission gear-tooth mesh frequency.

Figure 14b shows the transfer function identified for flap actuator voltage to normal balance load from a 0-80 Hz collective sweep. Several features of the transfer function are noteworthy. First, several rotor modal

frequencies are clearly visible, at approximately 1, 2.7, 3.5, 4.3, 7.0, and 10.2 per rev. Second, the phase lag in the transfer function is 900 deg over the frequency range from 0-12/rev. The large increase in phase lag with frequency has been seen in other actively controlled rotors [11]. This large phase delay in the transfer function limits the achievable performance of feedback controllers.

In order to control the harmonic vibrations in the normal force, a feedback control law with balance normal load as the measurement signal, and the collective flap voltage as the control signal is used. It targets the first five harmonics of vibration, with a sum of individual components $K(s) = \Sigma\, lK_n(s)$, where n=1-5, and the controller constants are obtained from the transfer function.

Figure 14c shows the resulting closed-loop spectrum of the balance normal force. The spectrum is almost identical to the spectrum in the open-loop case (Fig. 14a), except that the impulses in the spectrum corresponding to the first five harmonics are completely absent, which is to be expected, since the feedback control K(s) is infinite at those harmonics. Harmonic load values are obtained by summing the energy in the spectrum in a narrow frequency range (±0.5/rev) and l converting it to rms vibration levels. The dominant vibratory harmonic (1/rev) is reduced in magnitude by 98%, and 4/rev and 5/rev are reduced in magnitude by 90%. The overall reduction of harmonic vibration (of the first five harmonics) is 95%. Further, the total reduction in the normal force vibratory loads (including both harmonic and broadband vibration) over the range 0.5–5.5/rev is 84.5%.

Figure 15 shows the normal force and vibration index for baseline (0V) and five closed-loop controllers for normal force (NF) at =0.3, α=-9.1 deg. The three controllers for 1-5P use different transfer function and time constants. Harmonic load values are obtained from the time history averaged over one rotor revolution. Result show that that the controlled normal force components 1-5P are almost entirely eliminated, with reductions of 80% for 5P, 98% for 1P and 73% for the rms value of all harmonics. Corresponding results for the vibration index, including all five hub loads, are less impressive, with no reduction at 5P, 29% at 1P and 26% for rms. The uncontrolled normal force harmonics 6-9P appear unaffected, whereas the 10P harmonic increases slightly. The two controllers for 10P use different time constants. Results for normal force show good reduction of the 10P normal force when using the first controller (T=5) and excellent reduction of 98% when using the more aggressive controller (T=1). Again uncontrolled harmonics remain essentially unchanged. Surprisingly, the 10P vibration index is reduced by 76% (T=1).

Closed-loop active flap control of vibratory normal force using CTHHC was extremely effective, reducing harmonics 1-5P by 95% for both the level flight and descent condition. Control of vibratory roll moment in descent and pitch moment in level flight was shown to be slightly less effective, reducing harmonics 1-5P by 68% and 73%, respectively [32].

Closed-loop, simultaneous control of multiple loads using discrete time HHC or an advanced, discrete time controller that takes blade-to-blade dissimilarities into account [37] was planned for this entry, but no data was acquired in the available time.

Control Power

Control power from the active flaps was evaluated by applying equivalent steady-state collective, lateral, or longitudinal cyclic flap deflections and observing the resulting changes in normal force, roll, and pitch moment. Flap deflections were generated using a virtual swashplate (VSP), i.e. software mixing for flap inputs on each blade, or by applying 0P for collective 1P/90˚ for roll and 1P/180˚ for pitch inputs (IBC). Results for position control flap inputs, both VSP and IBC, and comparable swashplate inputs were obtained at =0.2 for level flight and descent, and for level flight at =0.3.

Figure 16 shows that the active flap generates substantial changes in lift and hub moments at =0.3. Thrust decreased by 1500 lb when moving the flaps collectively down from -3 to +3 deg. In comparison, thrust increased by 2700 lb when raising rotor collective pitch from -1 to +1 deg relative to the trimmed position. Similarly, roll moment increased by 15000 in-lb for flap inputs and 23500 in-lb for swashplate inputs. Pitch moment increased by 33700 in-lb for flap inputs and 45000 in-lb for swashplate inputs. These results indicate substantial control power from the active flaps. This is particularly noteworthy since the test stand has a very stiff control system (blade torsion mode near 6/rev), thus limiting the flap's l moment l control l effectiveness (servo effect) and resulting blade pitching motion. On the flight vehicle, with a much lower control system stiffness, active flap effectiveness can be expected to increase significantly [34].

Data was also acquired from multiple frequency sweeps over a 0-9 Hz range and is being evaluated to assess potential improvements in helicopter handling qualities with high rate active flap actuators.

Rotor Smoothing

Rotor smoothing, or blade tracking, was evaluated making steady-state inputs to individual flaps, either flap 1 or 2, using position control to move the active flap down from -3 to +3 deg in 1 deg steps. Since no direct measurement of blade track was available, the effectiveness of the active flap for rotor smoothing was assessed by considering the mean thrust and 1/rev roll and pitch moments resulting from the rotating lift force due to flap deflections on one blade. Results were obtained in hover, =0.2, α=2°, and =0.3, α=-9.1°.

Changes in hub loads from deflecting a single flap are shown in Figure 17. Figure 17a shows that mean thrust decreases by 450 lb and sin1P roll and cos1P pitch moment increase by 4000 in-lb when moving the flap on blade 1 down from -3 to 3 deg. This corresponds to about 7.5% of the nominal rotor thrust and 10% of the rotor balance oscillatory moment limit loads. Figure 17b shows the roll moment sine and cosine 1/rev components for three tunnel speeds, when moving flap 1. Clearly, the active flap effectiveness increases considerably with tunnel velocity; little effect is seen in hover. Also shown are results when moving flap 2, for the =0.3 case. lThe phase relationship indicated by the data properly reflects that blade 2 follows blade 1 by 72 deg in azimuth.

Results show that, as customary, pitch link adjustments should be used for track changes in hover. However, measured thrust changes and observed blade track changes due to flap inputs also indicate that use of active flaps for rotor smoothing in forward flight appears to be feasible.

Rotor Performance

A limited evaluation of rotor performance was conducted, considering two aspects. As noted before, when the active flap motion is not controlled (open-loop, 0V) the flaps experience considerable deflections and some blade-to-blade variations in flap response. While the blade-to-blade variations did show a reduction in BVI noise when compared to the case with flap position controlled to 0 deg (BVISPL lowered by more than 2dB) [30], the opposite was expected for performance.

Rotor performance comparison for 0 deg and 0V control is shown in Figure 18a for a thrust sweep in level flight at =0.3, α=-9.1 deg. Results are presented for the rotor lift coefficient versus power coefficient, both normalized by thrust-weighted solidity. In this case the rotor was trimmed at 0deg but not retrimmed for 0V. It is seen that the uncontrolled flap case carries a 1% performance penalty, i.e. lower rotor lift at the same power, for nominal and higher thrust values.

Of particular interest is the use of active flap control to potentially improve rotor performance. Two/rev active flap inputs were made at 1.5 deg amplitude and varying phase at =0.3, α=-9.1 deg and two thrust settings, C_T/σ 1 =0.075 and 0.09. In this case the rotor was trimmed at each test point. Results are presented for the rotor lift-to-drag ratio L/D = L / (P/V-D_p), where D_p is the parasite drag which is obtained from the propulsive force.

Figure 18b shows the rotor lift-to-drag ratio L/D as a function of flap input phase. Results for the baseline case (0deg) before and after the 2P phase sweeps are shown at 10 and 350 deg phase, respectively, for clarity. Not unexpectedly, the results raise questions regarding data consistency and repeatability. However, comparing the results from 2P flap inputs with the 2P averaged L/D for each thrust condition, there is a clear trend. Higher L/D is seen at 0-180 deg phase, and lower L/D at 180-360 deg phase. The difference between L/D at 90 and 270 deg is about 4%. Thus, a definite cause-effect relationship between 2/rev flap inputs and rotor performance is seen. Ignoring the outlier point at 60 deg phase, a 1% increase in L/D versus baseline is seen around 90 deg phase. Such a small change may be within the measurement accuracy, but the change is in the right direction and consistent with prediction [20].

CONCLUSIONS

A wind-tunnel test of the SMART active flap rotor was conducted in the 40- by 80-foot wind tunnel anechoic test section of the NFAC at NASA Ames. Loads, performance, and acoustic data were acquired in support of validating high-fidelity physics-based CFD-CSD rotor-noise prediction tools. The effectiveness of the active flap control on noise and vibration was conclusively demonstrated. Results show reductions in blade-vortex interaction (BVI) and in-plane noise as well as vibratory hub loads. Noise reductions up to 6dB, as well as vibratory hub load reductions of about 80% were measured. Trailing-edge flap deflections were controlled with less than 0.2 deg rms error for commanded harmonic profiles of up to 3 deg amplitude. The impact of the active flap on control power, rotor smoothing, and aerodynamic performance was also demonstrated. Finally, the reliability of the flap actuation system was successfully proven in more than 60 hours of wind-tunnel testing. Specific conclusions are as follows.

1. Both CTHHC and HHC were effective in controlling active flap position, using position feedback and applying individual control to each flap. When commanding zero deflection, flap deflections were within 0.12 deg for all speeds tested. When

commanding harmonic deflection profiles, the rms error was less than 0.2 deg.

2. Data for the validation of physics-based aero-acoustic prediction codes was successfully acquired at three test points. Blade loads were too high for the high-speed condition at 155 knot to exercise the specified flap deflection schedule, however, baseline data (with zero degree flap deflection) was acquired.
3. Reductions in BVI noise in descending flight and in-plane noise in level flight were demonstrated using active flap position control with single harmonic inputs. The best flap deflection profiles were determined through systematic variation of input phase, frequency, and amplitude. Both BVI and in-plane noise reduction incurred higher vibratory hub loads.
4. BVISPL reductions at the baseline rotor BVI hot spot varied between 3.5-6 dB at =0.15, and 3-5 dB at =0.165. At =0.2 smaller reductions of up to 3 dB were measured under the rotor disk. In all three cases 1.5 deg flap amplitude gave the best reductions.
5. In-plane noise reductions of up to 6 dB LFSPL were measured at =0.3, with a best active flap command of 1.3˚/4P/180˚.
6. Vibratory hub load reduction was demonstrated using the CTHHC algorithm for feedback control of one hub load at a time. Control of vibratory normal force was very effective, reducing harmonics 1-5P by 95% for both the level flight and descent condition. Control of vibratory roll moment in descent and pitch moment in level flight was shown to be slightly less effective, reducing harmonics 1-5P by 68% and 73%, respectively.
7. Steady-state flap inputs resulted in thrust and hub moment changes, and provided a measure of the control power available from the flaps. Hub load changes were substantial, especially considering the very stiff control system of the test stand which limited the flap's moment control effectiveness.
8. Rotor smoothing was evaluated through steady-state inputs to a single flap. Results indicated that it may be feasible to use flaps for in-flight blade tracking.
9. Rotor performance as measured by rotor L/D was affected by 2/rev flap inputs at =0.3. L/D increased at 90˚ and decreased at 270˚ phase, demonstrating the potential of the active flaps to improve performance. A 1% increase in L/D versus baseline was deemed too small to reach definitive conclusions.

ACKNOWLEDGEMENTS

Funding for the wind tunnel test was provided by DARPA as part of the Helicopter Quieting Program and by the NASA Subsonic Rotary-Wing program. The valuable contributions of the many dedicated staff members at Boeing, NASA, Army, DARPA, Air Force, MIT, UCLA, and University of Maryland are gratefully acknowledged. In particular, the authors would like to thank Mr. Daniel Newman, Dr. William Warmbrodt, and Dr. Ram JanakiRam for their support and many helpful discussions. Special thanks go to the authors of the companion papers, Drs. Ben Sim, Ram JanakiRam, and Steven Hall for sharing their material. Thanks also go to Mr. Roger Smith for his evaluation and assessment of SMART rotor performance.

REFERENCES

1. Wood, E.R., Powers, R.W., Cline, J.H., and Hammond, C.E., "On Developing and Flight Testing a Higher Harmonic Control System," JAHS, Vol. 30, No. 1, January 1985.
2. Polychroniadis, M., and Achache, M., "Higher Harmonic Control: Flight Tests of an Experimental System on SA 349 Research Gazelle," AHS 42nd Annual Forum, 1986.
3. Splettstoesser, W. R., Schultz, K. J., van der Wall, B. G., Buchholz, H., Gembler, W. and Niesl, G., "The Effect of Individual Blade Control on BVI Noise- Comparisons of Flight Test and Simulation Results', 24th European Rotorcraft Forum, Marseilles, France, 1998.
4. Bebesel, M., Roth, D., Pongratz, R., "Reduction of BVI Noise on Ground – In-flight Evaluation of Closed-Loop Controller," 28th European Rotorcraft Forum, Bristol, UK, Sept. 2002
5. Roth, D., "Advanced Vibration Reduction by IBC Technology," 130th European Rotorcraft Forum, Marseille, France, Sept. 2004.
6. Kessler, C., Fuerst, D., and Arnold, U.T.P., "Open Loop Flight Test Results and Closed Loop Status of the IBC System on the CH-53G Helicopter," AHS 59th Annual Forum, Phoenix, AZ, May 2003.
7. Arnold, U.T.P., "Recent IBC Flight Test Results from the CH-53G Helicopter," 129th European Rotorcraft Forum, Friedrichshafen, Germany, Sept. 2003.
8. Dieterich, O., Enenkl, B., and Roth, D., "Trailing Edge Flaps for Active Rotor Control – Aeroelastic Characteristics of the ADASYS Rotor System," AHS 62nd Annual Forum, Phoenix, 2006.
9. Konstanzer, P., Enenkl, B., Aubourg, P., Cranga, P., "Recent Advances in Eurocopter's passive and active vibration control," AHS 64th Annual Forum, Montreal, Canada, 2008.
10. Koratkar, N.A., and Chopra, I., "Wind Tunnel Testing of a Mach-Scaled Rotor Model with Trailing Edge Flaps," AHS 57th Annual Forum, Alexandria, VA, 2001, pp.1069-1099.
11. Fulton, M.V., and Ormiston, R.A., "Small-Scale Rotor Experiments with On-blade Elevons to Reduce Blade Vibratory Loads in Forward Flight," AHS 54th Annual Forum, Washington, DC, 1998.

12. Prechtl, E., and Hall, S.R., "Closed-Loop Vibration Control Experiments on a Rotor with Blade Mounted Actuation," 41st AIAA SDM Conference, AIAA-2000-1714, Atlanta, GA, April 2000.
13. Derham, R., Weems, D., Matthew, M., and Bussom, R., "The Design Evolution of an Active Materials Rotor," AHS 57th Annual Forum, Washington, DC, 2001.
14. Wilbur, M. L., Mirick, P. H., Yeager Jr., W. T., Langston, C. W., Cesnik, C. E. S., and Shin, S. J., "Vibratory Loads Reduction Testing of the NASA/Army/MIT Active Twist Rotor," AHS 57th Annual Forum, Washington, DC, May 9-11, 2001.
15. Crozier, P., et al, "Wind-Tunnel Tests of a Helicopter Rotor with Active Flaps," 32nd European Rotorcraft Forum, Mastrich, Netherlands, 2006.
16. Nitzsche, F., at el, "The SHARCS Project: Smart Hybrid Active Rotor Control System for Noise and Vibration Attenuation of Helicopter Rotor Blades," 31st European Rotorcraft Forum, Florence, Italy, 2005.
17. Hasegawa Y., Katayama N., Kobiki N., Nakasato E., Yamakawa E., Okawa H., "Experimental and Analytical Results of Whirl Tower Test of ATIC Full Scale Rotor System," AHS 57th Annual Forum, Washington, DC, May 9-11, 2001.
18. Straub, F.K., et al, " Development and Whirl Tower Test of the SMART Active Flap Rotor," SPIE Conf. on Smart Materials and Structures, San Diego, 2004.
19. Fulton, M.V., "Aeromechanics of the Active Elevon Rotor," AHS 61st Annual Forum, Grapevine, TX, 2005.
20. Yeo, H., "Assessment of Active Controls for Performance Enhancement," AHS 62nd Annual Forum, Phoenix, AZ, 2006.
21. Johnson, W., "CAMRAD II, Comprehensive Analytical Model of Rotorcraft Aerodynamics and Dynamics," Release 4.7, Johnson Aeronautics, Palo Alto, 2008.
22. Patt, D., Liu, L., and Friedmann, P.P., "Rotorcraft Vibration Reduction and Noise Prediction Using a Unified Aeroelastic response Simulation," JAHS Vol 50(1), Jan. 2005.
23. Liu, L., Friedmann, P.P, Kim, I., and Bernstein, D.S., "Simualtenous Vibration reduction and Performance Enhancement in Rotorcraft Using Actively Controlled Flaps," AHS 62nd Annual Forum, Phoenix, AZ, May 2006.
24. Ananthan, S., and Baeder, J.D., "Prediction and Validation of Loads on Bearingless Rotors Using a Coupled CFD-CSD Methodology," AHS 64th Annual Forum, Montreal, May 2008.
25. Kottapalli, S, and Straub, F.K., Correlation of SMART Active Flap Rotor Loads," AHS 65th Annual Forum, Grapevine, TX, May 2009.
26. Straub, F. K., and Kennedy, D. K., "Design, Development, Fabrication and Testing of an Active Flap Rotor System", AHS 61st Annual Forum, Grapevine, Texas, June 2005.
27. Straub, F. K., and Hassan, A. A., "Aeromechanic Considerations in the Design of a Rotor with Smart Material Actuated Trailing Edge Flaps," AHS 52nd Annual Forum, Washington DC, June 1996.
28. Hall, S.R., Tzianetopoulou, T., Straub, F.K., and Ngo, H., "Design and Testing of a Double X-Frame Piezoelectric Actuator," SPIE Conf. on Smart Structures and Materials, Newport Beach, CA, March 2000.
29. Jacklin, S. A., Lau, B. H., Nguyen, K. Q., Smith, R. L. and McNulty, "Full-Scale Wind Tunnel Test of the McDonnell Douglas Five-Bladed Advanced Bearingless Rotor: Performance, Stability, Loads, Control Power, Vibration and HHC Data," AHS Aeromechanics Specialists Conference, San Francisco, CA, Jan. 1994.
30. JanakiRam, R.D., Sim, B.W., Kitaplioglu, C., and Straub, F.K., "Blade-Vortex Interaction Noise Characteristics of a Full-Scale Active Flap Rotor," AHS 65th Annual Forum, Grapevine, TX, May 2009.
31. Sim, B.W., JanakiRam, R.D., Barbely, N.L., and Solis, E., "Reduced In-Plane, Low Frequency Noise of an Active Flap Rotor," AHS 65th Annual Forum, Grapevine, TX, May 2009.
32. Hall, S.R., Anand, V.R., Straub, F.K., and Lau, B.H., "Active Flap Control of the SMART Rotor for Vibration Reduction," AHS 65th Annual Forum, Grapevine, TX, May 2009.
33. Molusis, J.A., Hammond, C.E., and Cline, J.H., "A Unified Approach to the Optimal Design of Adaptive and Gain Scheduled Controllers to Achieve Minimum Helicopter Vibrations," AHS 37th Annual Forum, New Orleans, May 1981.
34. Straub, F.K., Charles, B.D., "Comprehensive modeling of rotors with trailing edge flaps," AHS 55th Annual Forum, Montreal, May 1999, JAHS Vol 46(3), July 2001.
35. Straub, F.K., and Anand, V.R, "Whirl Tower Test and Analysis of the SMART Active Flap Rotor," Presented at the AHS 63rd Annual Forum, Virginia Beach, VA, 2007.
36. Shaw, J., J., "A Feasibility Study of Helicopter Vibration Reduction by Self-Optimizing Higher Harmonic Blade Pitch Control," Master's thesis, MIT, Dept. of Aeronautics and Astronautics, 1967.
37. Roget, B., and Chopra, I., "Individual Blade Control Methodologies for a Rotor with Dissimilar Blades," JAHS, Vol 48(3), July 2003, pp.176-185.

Table 1: SMART Rotor Characteristics

Rotor blade	modified MD900
Hub type	bearingless (MD900)
No. of blades	5
Rotor Diameter	33.85 ft (R=203.1in)
Rotor Speed	392 rpm
Tip Speed	695 ft/s
Chord	10 in
Airfoils	HH-10, t/c=12%, to 0.74R HH-06, t/c=9.5%, from 0.84R
Tip Sweep	parabolic LE, from 0.93R; 22deg at tip
Tip Taper	2:1, straight trailing edge
Twist	-10 deg
Torsion frequency	5.8/rev

Table 2: Flap Characteristics

Radial station	150 –"186 in
Span length	36 in
Chord length	3.5 in ($c_f + c_o$)
Hinge location	75% of blade chord
Flap twist axis	1.0 in aft of flap LE
Control horn length	0.75 in
Max. flap angle	± 6 deg
Flap weight	1.26 lbs

Table 3: 2X-Frame actuator characteristics

Blocked force	113 lb
Free stroke	0.081 in
Maximum work	2.28 in-lb
Voltage, max (nom)	475 ± 725V (400±500V)
Weight	2.16 lb
Specific work	1.1 in-lb/lb

Table 4: MD900 / SMART Blade Mass Properties

	MD900	SMART
Weight (lbs.)	39.16	44.22
Span Moment (in.-lbs.)	4550	5244
CG chordwise	27.3%	26.7%

Table 5: Blade Frequencies, SMART versus MD900

Analysis, cyc/rev Flat pitch, vacuum			Measured, Hz Free-free blade		
Mode	SMART	MD900	Mode	SMART	MD900
1C	0.58	0.59			
1F	1.05	1.05	1F	6.56	6.63
2F	2.8	2.7	2F	18.1	18.9
2C	4.4	4.5	3F	36.8	36.6
3F	4.6	4.7	1C	40.8	41.1
1T	6.4	6.0	1T	69.7	68.5
			1TEF	95.8	--

Table 6: Active flap test conditions

Objective	Condition	Velocity*, V, kt	Advance Ratio*, μ	Tip Mach # MT	Adv Tip Mach # MAT	Shaft Angle uncorrected α, deg	Blade Loading, CT/σ	Active Flap Control: Harmonic Number, n	Active Flap Control: Amplitude A, deg [V]	Active Flap Control: Phase φ, deg
Validation	1	123	0.3		0.805	-9.4	0.08	5	0, 2	90
	2	123	0.3		0.805	-9.4	0.08	3	0, 2	60
	3	155	0.375		0.852	-9.3	.07, (.075)	5	0, (1)	180
	4	83	0.2		0.746	0.9	0.075	2 & 5	0, 2 & 1	240 & 330
BVI Noise	1	62	0.15	0.623		4	0.075	2,3,4,5	1 - 2	sweep
(RPM=392)	2	68	0.165	0.617		1.8	"	3,4	1 - 2	"
	3	82	0.2	0.623		2	"	2,3,4,5	1 - 2.5	"
Inplane Noise	1	124	0.3	0.623	0.809	-9.1	0.075	2,3,4,5	1 - 2	"
Vibration	1	82	0.2	0.623		2	0.075	2,3,4,5,6	250V	sweep
	2	"	"	"		"	"	Closed Loop: NF 5,1,1-5P; RM 5,1,1-5P		
	3	124	0.3	"		-9.1	"	2,3,4,5,6	250V	sweep
	4	"	"	"		"	"	Closed Loop: 1-5P, 10P; PM 1-5P		
Control Power	1	82	0.2	0.623		-5.5	0.075	0,1	-3 to 3	0,90
	2	"	"	"		2	"	"	"	"
	3	124	0.3	"		-9.1	"	"	"	"
Rotor Smoothing	1	0	0	0.623		-10	0.028	0	A1=-3 to +3	
	2	82	0.2	"		2	0.075	"	"	
	3	124	0.3	"		-9.1	"	"	"	
	4	"	"	"		"	"	"	A2=-3 to +3	
Performance	1	82	0.2	0.623		2	0.075	n/a	0V, 0	
	2	124	0.3	"		-9.1	0.075	"	0V, 0	
	3	"	"	"		"	0.075	2	0, 1.5	sweep
	4	"	"	"		"	0.09	"	"	"

NF - normal force, RM - roll moment, PM - pitch moment, [alternate units], (target condition, not achieved)
* Condition is set to value shown in large type font

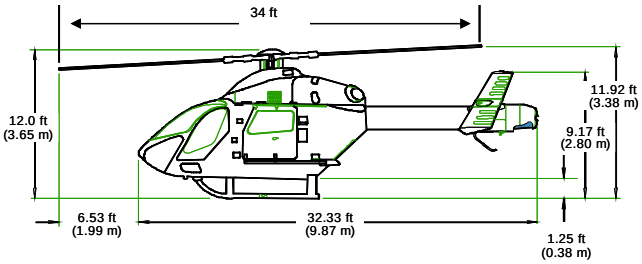

Figure 1a: MD900 Explorer

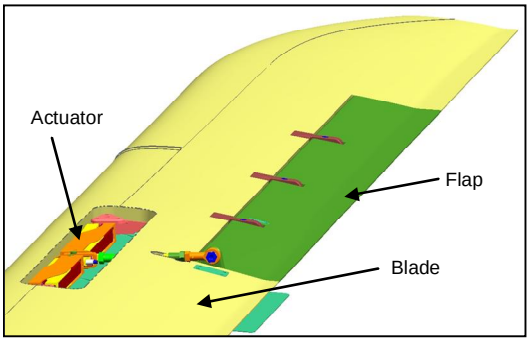

Figure 1b: SMART blade with embedded piezoelectric actuator and trailing edge flap

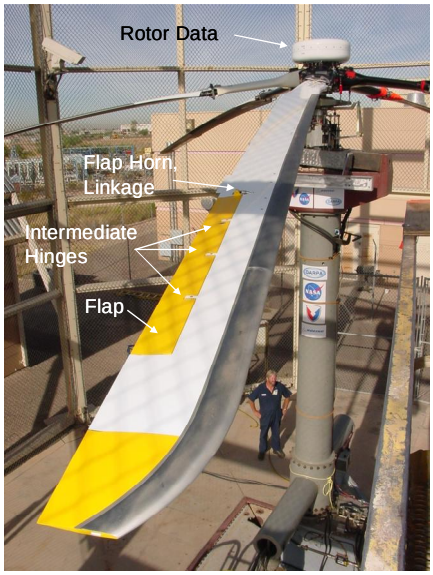

Figure 1c: SMART rotor blade on whirl tower

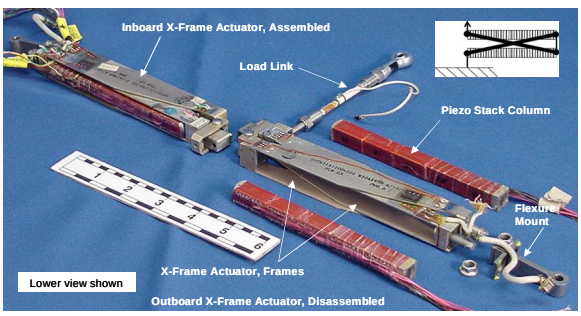

Figure 1d: 2x-Frame piezoelectric actuator

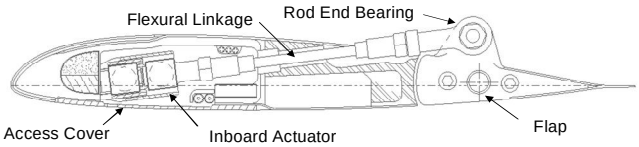

Figure 1e: SMART Blade, flap, actuator cross-section

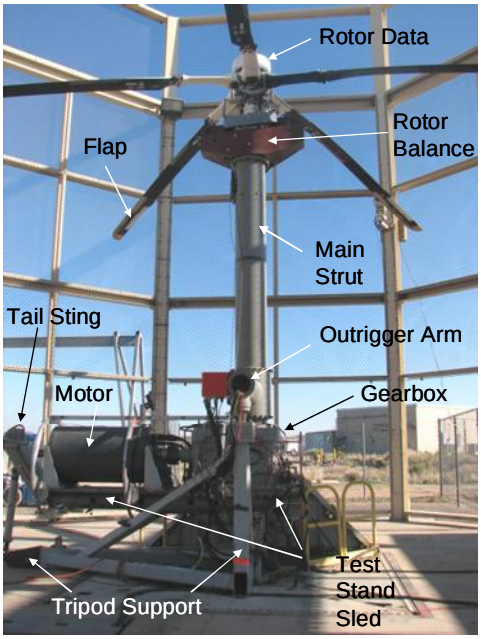

Figure 2: System integration test at whirl tower

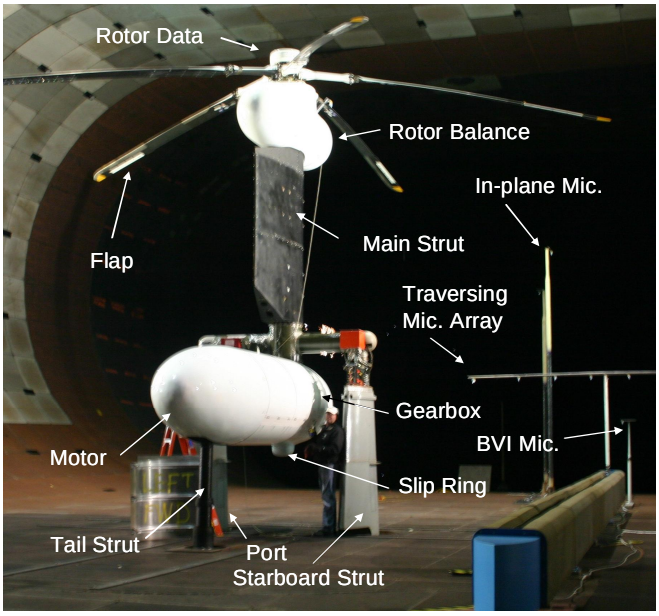

Figure 3a: SMART rotor in the NFAC 40- by 80-foot wind tunnel (looking upstream)

Figure 3b: Close-up view of the SMART rotor, blade, and flap in the tunnel

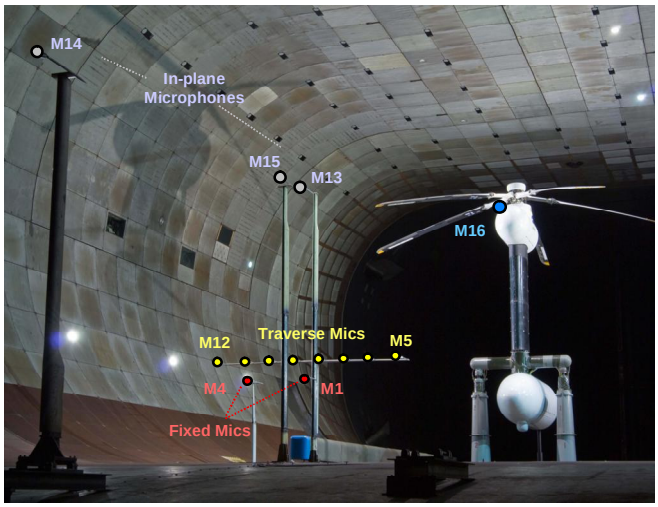

a) SMART rotor in 40- by 80-foot anechoic test section and microphone configuration (looking downstream)

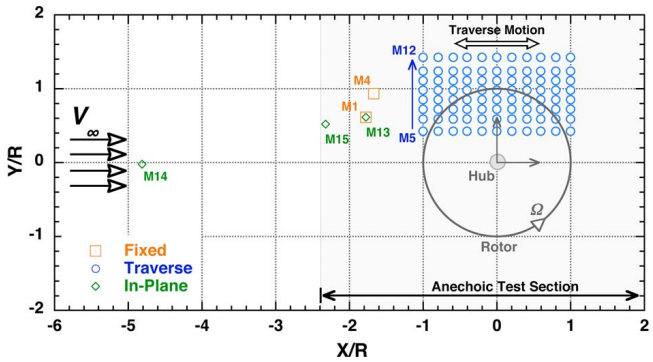

b) Microphone layout (top view)

Figure 4. Acoustic test setup: a) SMART rotor and microphone configuration, b) microphone layout

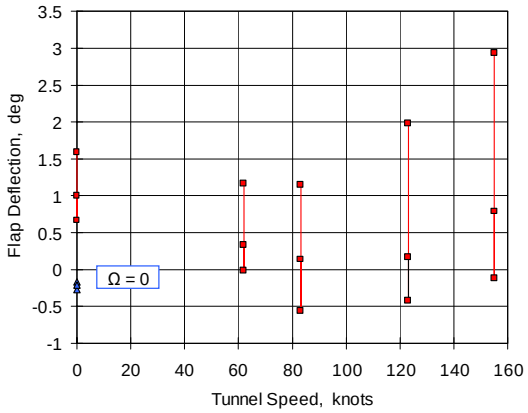

Figure 5a: Active flap deflection versus speed, open-loop flap with 0 Volt applied

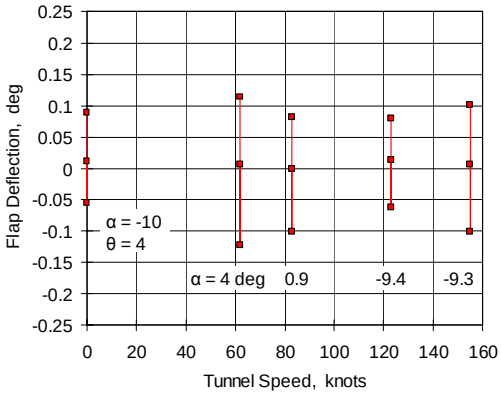

Figure 5b: Active flap deflection versus speed, closed-loop flap position control with 0deg command

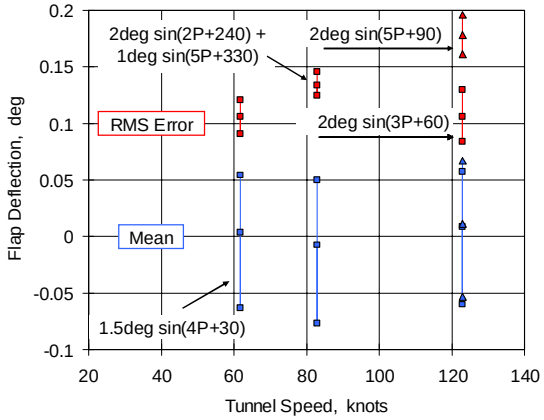

Figure 5c: Active flap mean deflection and RMS error versus speed, closed-loop flap position control with four harmonic commands

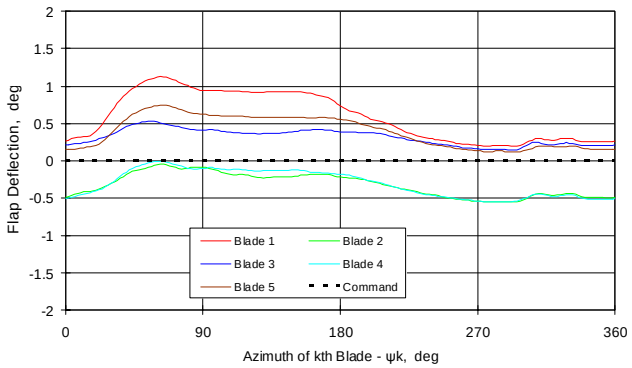

Figure 6a: Active Flap deflection versus azimuth at 83 knots, αδ= 0.89 deg, uncontrolled (0V)

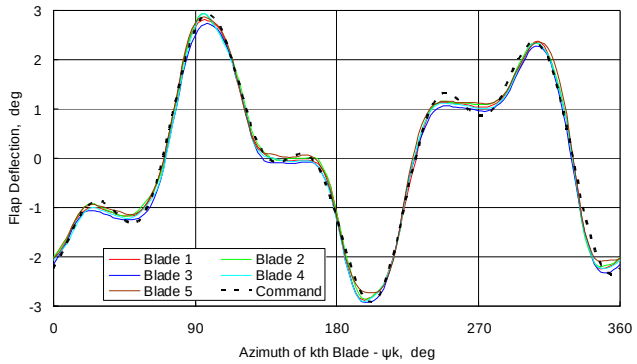

Figure 6b: Active flap deflection versus azimuth at 83 knots, αδ= 0.89 deg, $_f$ = 1.5deg sin(2ψ+240) + 1deg sin(5ψδ+330)

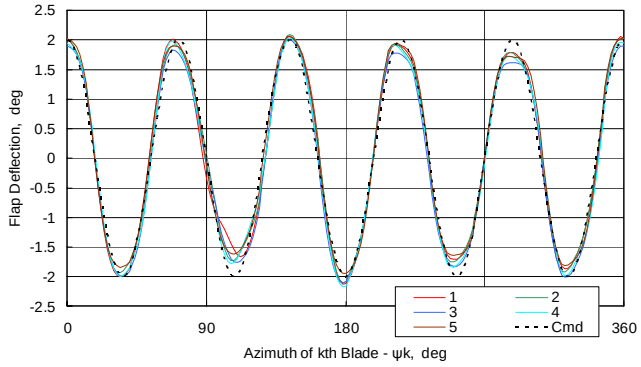

Figure 6c: Active flap deflection versus azimuth at 123 knots, αδ= -9.4 deg, $_f$ = 2 deg sin(5ψ+90)

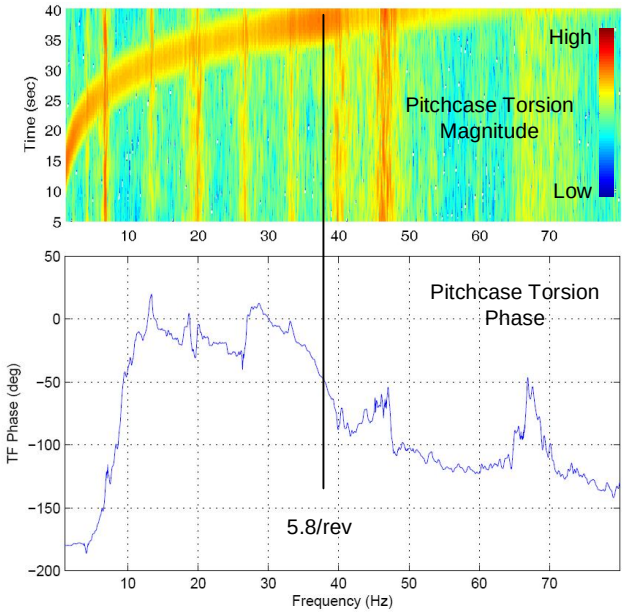

Figure 7: Pitchcase torsion magnitude (power spectral map, log scale) and phase (deg) from active flap frequency sweep; 200V collective, 0.2-80 Hz log sweep, hover, αδ= -10°, collective pitch = 4°

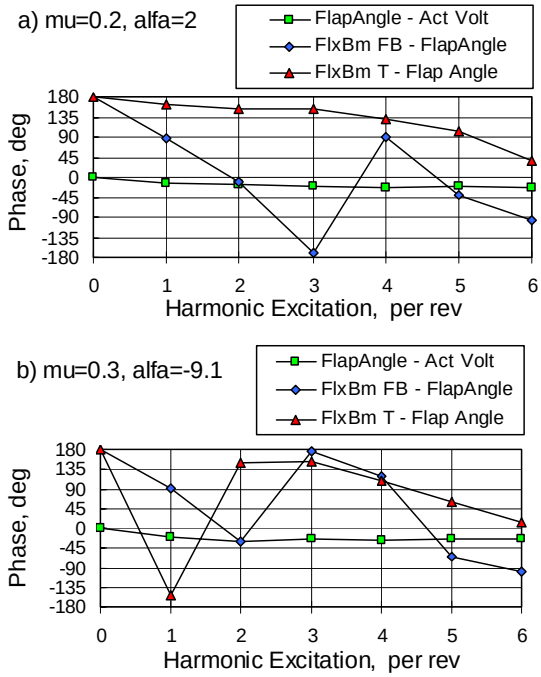

Figure 8: Phase relationships for excitation at rotor speed multiples; active flap vs voltage and flexbeam flap bending and torsion vs active flap

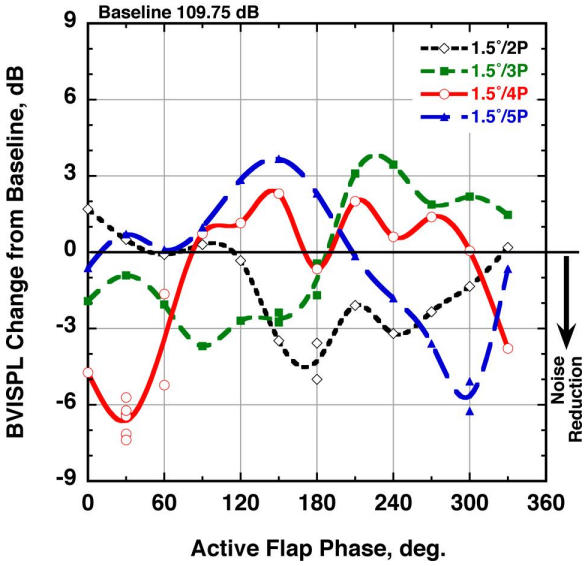

Figure 9: Effect of active flap excitation on BVISPL for Condition 1 (μ = 0.150, α = +4.0˚) at microphone M7 (traverse station: –120)

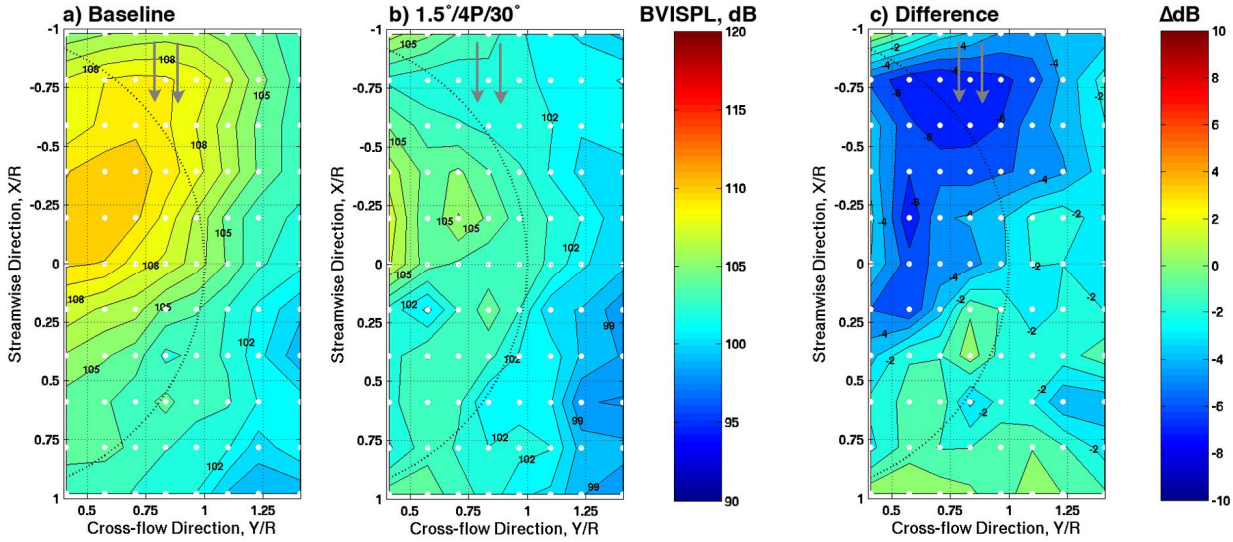

Figure 10a: BVISPL contours for baseline (0 deg) and active flap actuation (1.5˚/4P/30˚) for Condition 1 (μ = 0.150, α = +4.0˚)

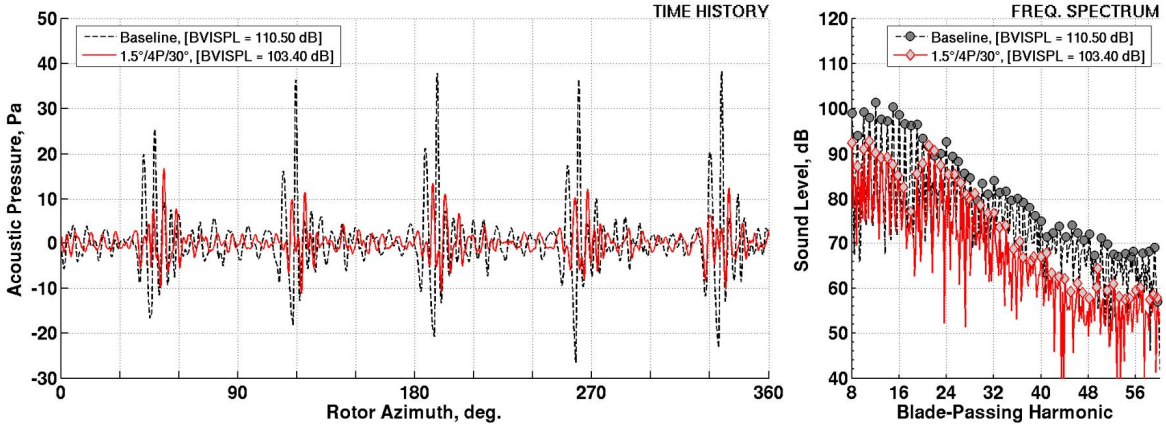

Figure 10b: Acoustic pressure time histories and spectral data for baseline (0 deg) and active flap actuation (1.5˚/4P/30˚) for Condition 1 (μ = 0.150, α = +4.0˚) at microphone M7 (traverse station: -120)

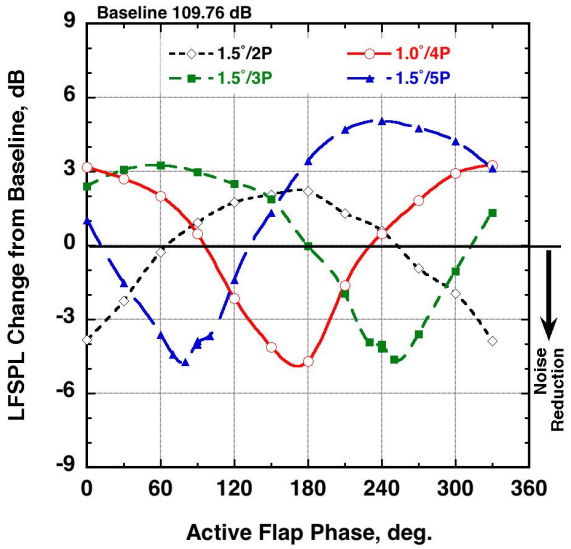

Figure 11a: Effect of active flap excitation frequency and phase on LFSPL at microphone M13; $\mu = 0.3$, $\alpha = -9.1^\circ$

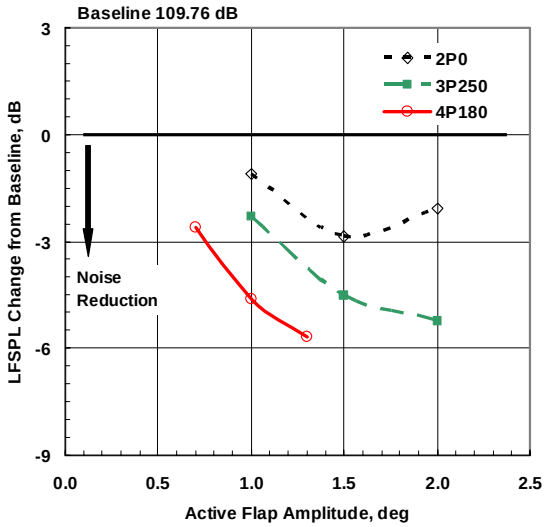

Figure 11b: Effect of active flap excitation frequency and amplitude for best"phase on LFSPL at microphone M13; $\mu = 0.3$, $\alpha = -9.1^\circ$

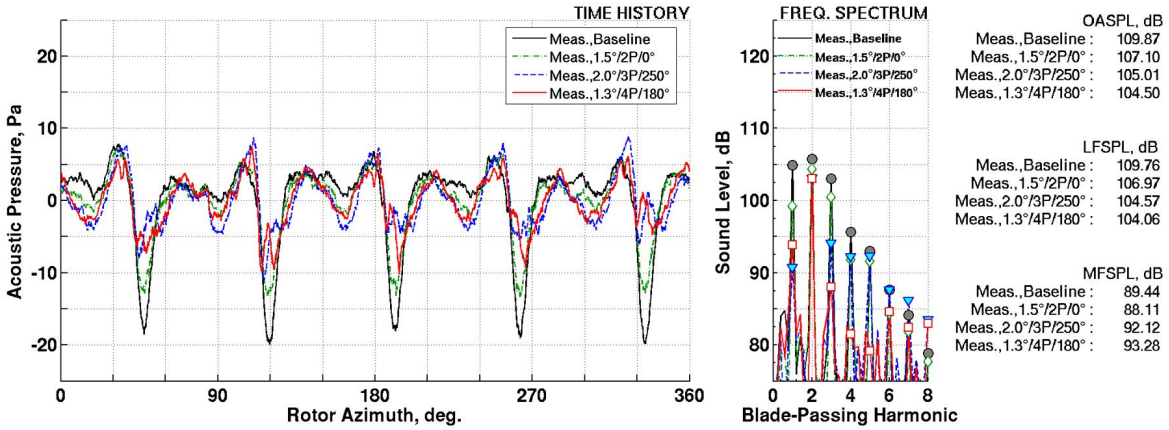

Figure12: Measured acoustic time histories and frequency spectra at best"phase, best"amplitude conditions (microphone M13): a) 1.5°/2P/0°, b) 2.0°/3P/250°, c) 1.3°/4P/180°; $\mu = 0.3$, $\alpha = -9.1^\circ$ (OASPL –overall SPL; MFSPL –medium frequency SPL, > 6th blade-passing harmonic)

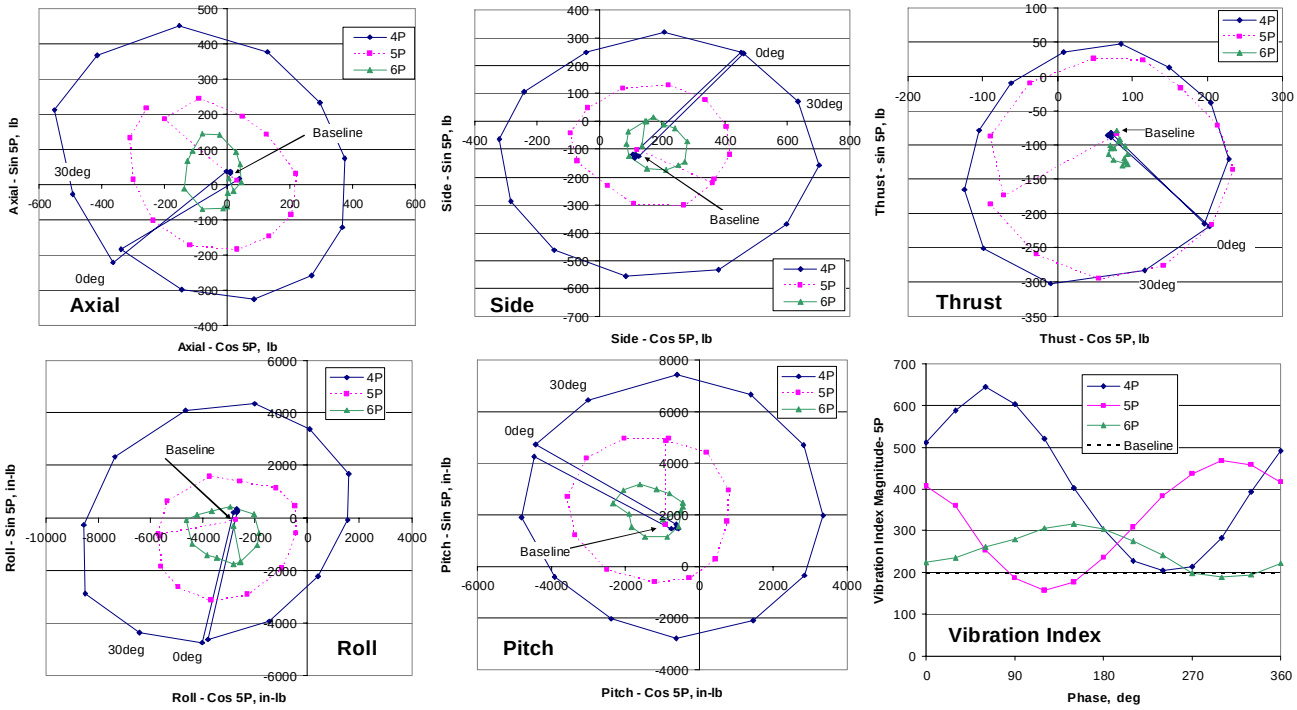

Figure 13: Vibratory hub loads (5P) for baseline case (0V) and open-loop active flap control phase with 250V amplitude at 4, 5, and 6P; $\mu = 0.3$, $\alpha\delta = -9.1^\circ$

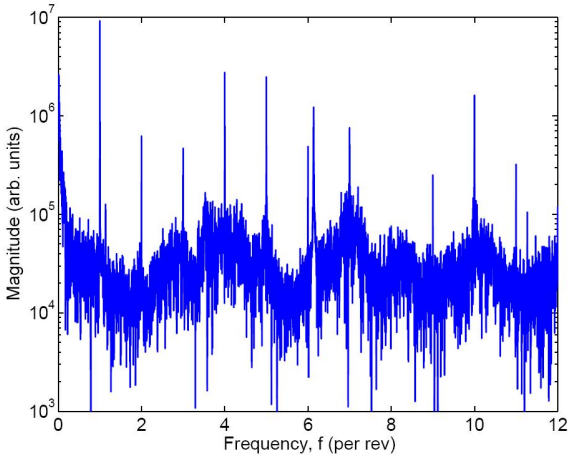

Figure 14a: Fast Fourier transform (spectrum) of balance normal force for open-loop case (0V); $\mu = 0.2$, $\alpha = 2^\circ$

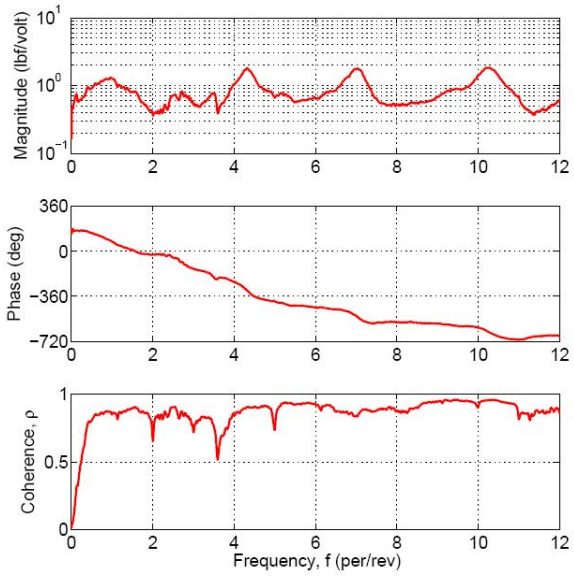

Figure 14b: Estimated transfer function from actuator voltage to balance normal force; 200V collective, 0-80 Hz linear sweep; $\mu = 0.2$, $\alpha = 2^\circ$

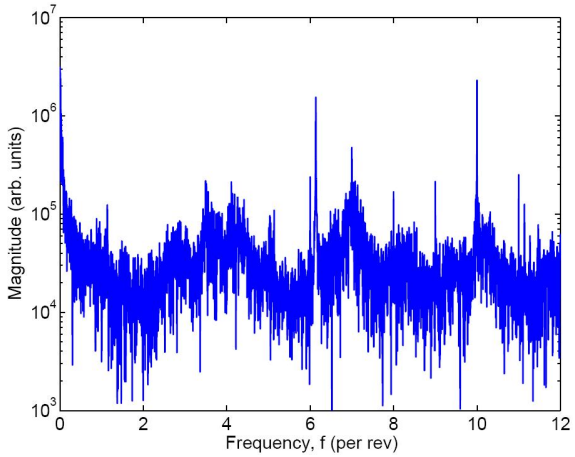

Figure 14c: Fast Fourier transform (spectrum) of balance normal force for closed-loop active flap control of normal force 1-5P; $\mu = 0.2$, $\alpha = 2^{\circ}$

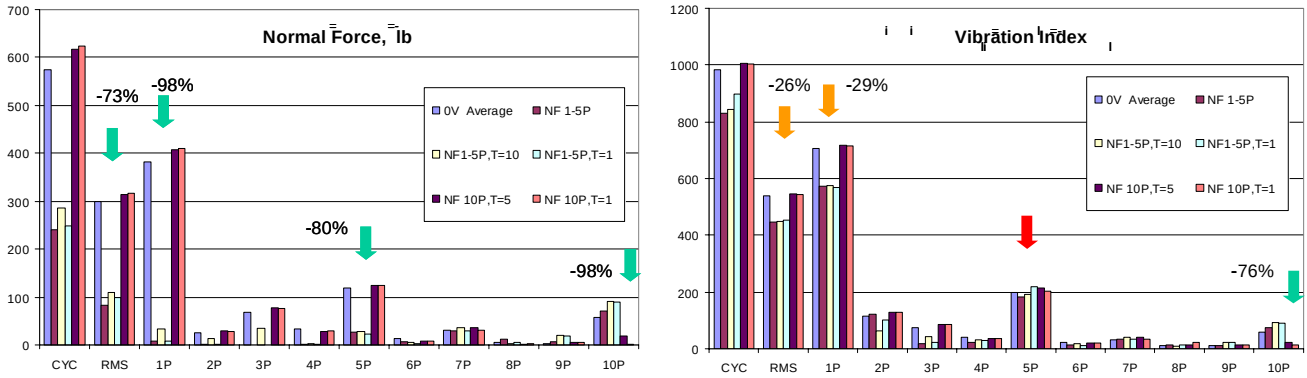

Figure 15: Vibratory hub normal force and vibration index for baseline case (0V) and closed-loop active flap control of normal force (NF); $\mu = 0.3$, $\alpha\delta = -9.1^{\circ}$

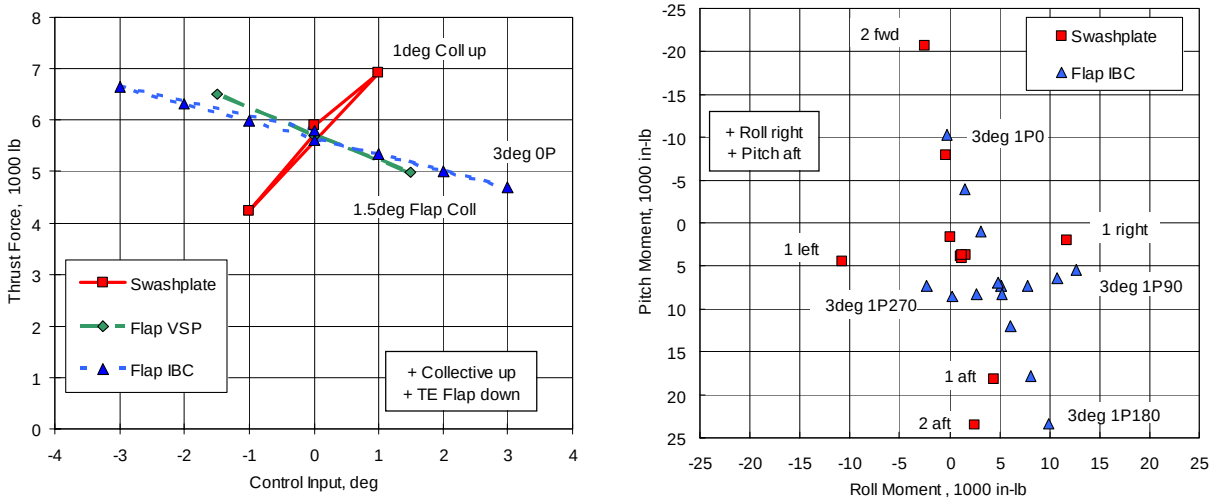

Figure 16: Control power: steady hub load changes from swashplate and active flap inputs; $\mu = 0.3$, $\alpha\delta = -9.1^{\circ}$
a) Thrust from collective inputs, and b) Hub moments from cyclic inputs

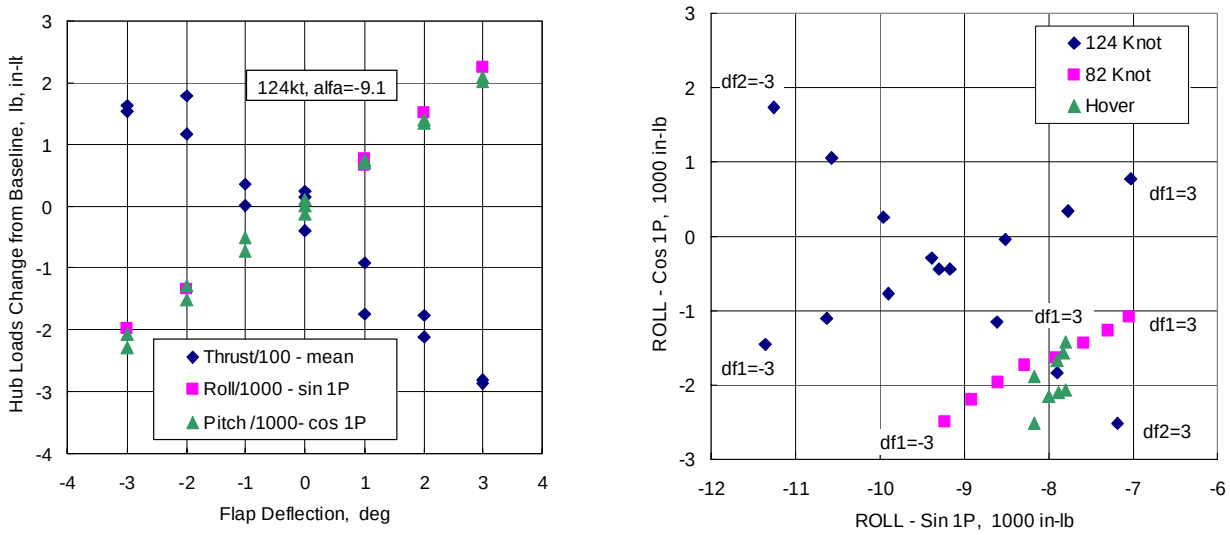

Figure 17: Rotor smoothing: hub load changes from steady inputs of -3 to +3 deg on a single active flap.
a) thrust (mean), roll moment (sin1P), and pitch moment (cos1P) relative to baseline with flap 1; $\mu = 0.3$, $\alpha = -9.1^{\circ}$;
b) roll moment (1P) with flap 1 or flap 2 (df1, df2); $\mu = 0$, $\alpha = -10^{\circ}$; $\mu = 0.2$, $\alpha = 2^{\circ}$; $\mu = 0.3$, $\alpha = -9.1^{\circ}$

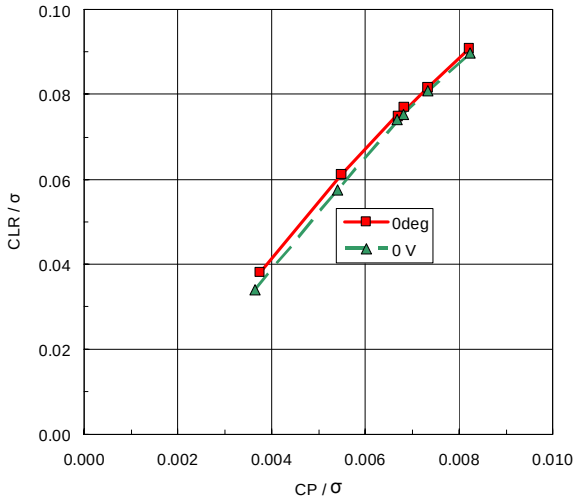

Figure 18a: Rotor performance with open-loop (0V) and active flap position control (0 deg); $\mu = 0.3$, $\alpha_{\delta=} -9.1^{\circ}$

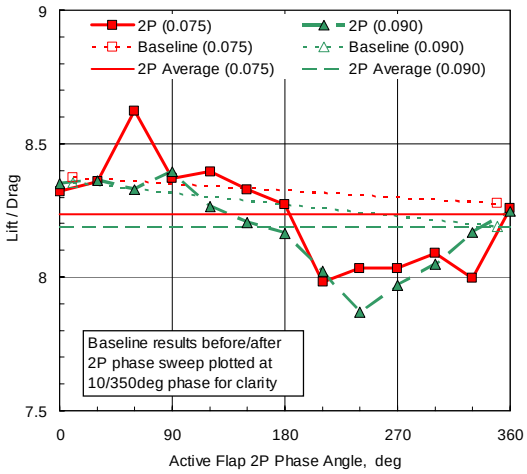

Figure 18b: Rotor performance with active flap inputs of 0 deg and 1.5 deg sin(2P + ϕ);
$\mu = 0.3$, $\alpha_{\delta=} -9.1^{\circ}$, $C_T/\sigma = 0.075, 0.09$